Molecular Modeling and Molecular Dynamics Simulations of Recombinase Rad51

Yuichi Kokabu and Mitsunori Ikeguchi*
Graduate School of Nanobioscience, Yokohama City University, Yokohama, Japan

ABSTRACT The Rad51 ATPase plays central roles in DNA homologous recombination. Yeast Rad51 dimer structure in the active form of the filament was constructed using homology modeling techniques, and all-atom molecular dynamics (MD) simulations were performed using the modeled structure. We found two crucial interaction networks involving ATP: one is among the γ-phosphate of ATP, K^+ ions, H352, and D374; the other is among the adenine ring of ATP, R228, and P379. Multiple MD simulations were performed in which the number of bound K^+ ions was changed. The simulated structures suggested that K^+ ions are indispensable for the stabilization of the active dimer and resemble the arginine and lysine fingers of other P-loop containing ATPases and GTPases. MD simulations also showed that the adenine ring of ATP mediates interactions between adjacent protomers. Furthermore, in MD simulations starting from a structure just after ATP hydrolysis, the opening motion corresponding to dissociation from DNA was observed. These results support the hypothesis that ATP and K^+ ions function as glue between protomers.

INTRODUCTION

Homologous recombination, in which DNA strands are exchanged between a pair of homologous sequences, is crucial for both the repair of damaged DNA and the maintenance of genomic diversity. The DNA strand exchange reaction in homologous recombination is mainly catalyzed by ATPases that are known as recombinases. The processes in the DNA strand exchange that involve recombinases are evolutionally conserved (1). After double-strand breaks in DNA, a free 3′ end of single-stranded DNA (ssDNA) is generated by a nuclease that degrades the 5′ end of the complementary strand. Recombinases bind to ssDNA and form a nucleo-protein filament called a presynaptic filament that searches for the homologous intact double-stranded DNA (dsDNA). Next, strand invasion of the ssDNA into dsDNA occurs, and DNA strands are subsequently exchanged between the ssDNA and dsDNA. Therefore, a presynaptic filament comprising recombinases and ssDNA is key in the DNA strand exchange reaction.

The recombinase protein family consists of Rad51 for eukaryotes, RadA for archaea, and RecA for bacteria. The primary sequence of Rad51 is more homologous to RadA than to RecA. The sequence identities between Rad51 and RadA and between Rad51 and RecA are ~40% and ~20%, respectively (2). All three recombinases share a core domain exhibiting ATPase activity. RecA has an additional C-terminal DNA-binding domain that is absent in Rad51 and RadA. In contrast, Rad51 and RadA have an extra N-terminal DNA-binding domain that is completely different from the C-terminal domain of RecA.

After the first report of an x-ray crystallographic structure of RecA (3), a number of recombinase structures have been reported for two decades (4–7). Electron microscopy (EM) studies revealed that the recombinase filament adopts two different forms; one is extended with a helical pitch of ~90–100 Å, and the other is compressed with a helical pitch of ~70–80 Å (4,8). The extended form is observed in the presence of DNA and ATP and corresponds to the active presynaptic form. In contrast, in the presence of ADP or in the absence of nucleotides, recombinases form the compressed inactive filament. Most of the crystal structures of RecA exhibit a helical pitch of ~70–80 Å, corresponding to the compressed inactive form. In those inactive structures, the nucleotide-binding site is located at the side of the filament, not at the interface between protomers. An exception is a recently determined structure of the DNA-RecA complex, which adopts the extended active form (9). In the structure, ATP (actually, ADP and AlF_4 are bound in the crystal structure) is located at the interface of protomers and functions as glue connecting the RecA protomers in the recombinase filament. The phosphates of ATP are bound to the Walker A or P-loop motif of one protomer and to two lysine side chains of the other adjacent protomer (Fig. S1 in the Supporting Material). The recognition of the ATP γ-phosphate by two lysine residues of the adjacent protomer is similar to that of the arginine fingers of ATP synthase (10) and Ras-GAP complex (11). However, because the two lysine residues are specific for RecA (Fig. S1), Rad51 and RadA adopt another method for recognizing the ATP γ-phosphate.

Submitted September 11, 2012, and accepted for publication February 7, 2013.

*Correspondence: ike@tsurumi.yokohama-cu.ac.jp

Editor: Michael Feig.

0006-3495/13/04/1556/10 $2.00

http://dx.doi.org/10.1016/j.bpj.2013.02.014

The crystal structure of yeast Rad51 exhibits a significantly more extended form with a helical pitch of ~130 Å (12,13), which is unlikely to be the active form. In addition, no nucleotide is bound to the structure. Recently, using site-specific linear dichroism spectroscopy, a filament model of human Rad51 was constructed (14). Because this study focused on overall arrangements of Rad51 protomers in the filament, the ATP-binding site was not investigated in detail. Thus, at present, the recognition mechanism of ATP in Rad51 is not understood in a detailed fashion. In this study, we investigate ATP recognition in Rad51 using homology modeling and molecular dynamics (MD) simulations with explicit solvent. In homology modeling, we used a crystal structure of RadA (5) as a reference structure. The RadA crystal structures adopt a properly extended form with a helical pitch of ~90–100 Å, and either an ATP analog or ADP is bound to the interface of protomers (6). Depending on the solvent conditions, one or two potassium ions or one calcium ion is located in the vicinity of the ATP γ-phosphate (5–7). Therefore, in RadA, these cations are likely to act as the lysine finger in RecA. In this study, by referencing a monomeric structure in the yeast Rad51 crystal structure and the relative arrangement of protomers in the RadA crystal structure, we constructed a dimer model of yeast Rad51 as a minimal unit of an active form of the Rad51 filament. Next, multiple MD simulations were performed of the modeled structures under different conditions, including the presence or absence of cations in the vicinity of the γ-phosphate. We address the questions of what condition stabilizes the Rad51 filament, whether cations also play roles in recognition of the ATP γ-phosphate in Rad51, and what are other factors in the role of ATP as a glue connecting protomers. Finally, we discuss effects of ATP hydrolysis on the active form of the Rad51 filament.

METHODS

The yeast Rad51 dimer structure in the active form of the filament was modeled using the homology modeling techniques. For reference structures, the structures of a protomer and dimer were extracted from the crystal structure of the yeast Rad51 filament (PDBID: 3LDA) and the archaeal RadA filament (PDBID: 1XU4), respectively. Sequence alignments between Rad51 and RadA were performed using the program BLAST (Fig. S2) (15). The identity and similarity of the alignment were 40% and 59%, respectively. Because gap residues in the alignment (4%) were located at the surface far from the interface of the dimer, the insertions and deletions have little impact on the modeling. We compared the BLAST results with the alignment generated using ClustalX (16), T-COFFEE (17), and MUSCLE (18). All of the alignments were essentially the same, and the slight difference in the alignments (e.g., terminal residues) did not affect homology modeling. Thirty dimer structures were built with the program MODELER (19) using multiple templates, i.e., two monomeric Rad51 crystal structures, and a dimeric RadA crystal structure. Among the 30 built structures, we selected three candidate structures in which the side-chain configurations of the five important interface residues, D280, S192, R228, H352, and D374 resembled those of the RadA crystal structure and the side chain of R188 did not overlap with the ATP. From those candidates, we then chose the best structure in terms of the MODELER score function. The geometrical quality of the model evaluated using PROCHECK (20) was similar to that of the crystal structures (Table S1). ATP, magnesium, and potassium ions were inserted into the modeled Rad51 structure by referencing the RadA crystal structure.

The modeled structure of the yeast Rad51 dimer was subjected to all-atom MD simulations with explicit water. The conditions of the MD simulations are summarized in Table 1. All of the MD simulations were performed with the program MARBLE (21) using CHARMM22/CMAP for proteins (22), CHARMM27 for nucleotides and ions (23), and TIP3P for water (24) as the force-field parameters. Electrostatic interactions were calculated using the particle-mesh Ewald method. The Lennard-Jones potential was smoothly switched to zero over the range 8–10 Å. The symplectic integrator for rigid bodies was used for constraining the bond lengths and angles involving hydrogen atoms. The time step was 2.0 fs. The procedures of the MD simulations were as follows: The initial structures were immersed in a water box. K^+ and Cl^- ions were added to the systems such that the KCl concentration of the resulting system was 150 mM. The resulting systems contained ~66,000 atoms. For equilibration, the systems were gradually heated to 293 K for 100 ps under the NVT ensemble with constraints on the positions of solute atoms. Subsequent MD simulations were performed for 100 ps under the NPT ensemble using the same constraints. Next, the constraints on the L1 and L2 loops in Rad51 were gradually decreased over a period of 100 ps, and finally, the constraints on all other solute atoms were gradually removed over a period of 100 ps. After the equilibration, 100 ns product runs were performed at 1 atm and 293 K. Each simulation was repeated as shown in Table 1.

To analyze the opening motions in ADP-bound simulations, principal component analysis (PCA) was performed. First, structures in the trajectory of simulation $K^2N^{ATP}I^M$ were averaged, and snapshots of simulations $K^2N^{ATP}I^M$, $K^2N^{ADP+Pi}I^M$, and $K^2N^{ADP}I^M$ were aligned to the average structure using least square fits of the core domain of protomer A (see Fig. 1). A covariance matrix of the core domain of protomer B from the average structure was then calculated and diagonalized to obtain principal modes. Therefore, principal modes represent the major motions of protomer B relative to protomer A. To estimate how much principal modes resemble random diffusion, their cosine contents were calculated. Hess has shown that for random diffusion on a flat potential surface, the first few principal components are represented by cosines with the number of periods equal to half the principal component index (25). The cosine content c_i of principal component i is given by the following equation:

$$c_i = \frac{2}{T}\left(\sum_{t=1}^{T}\cos\left(\frac{i}{T-1}\pi t\right)p_i(t)\right)^2\left(\sum_{t=1}^{T}p_i^2(t)\right)^{-1}$$

where T is the length of the simulation, and $p_i(t)$ is the amplitude of the motion along principal mode i at time t. The cosine content is in the range from 0 (no similarity to a cosine) to 1 (a perfect cosine).

To complement the MD simulations, electrostatic energies of the modeled structures with different numbers of bound K^+ ions were

TABLE 1 Summary of MD simulations

Simulation	Number of K^+	Nucleotide	Initial structure	Simulation times	Repeat
$K^2N^{ATP}I^M$	2	ATP	Model	100 ns	2
$K^1N^{ATP}I^M$	1	ATP	Model	100 ns	2
$K^0N^{ATP}I^M$	0	ATP	Model	100 ns	3
$K^2N^{ADP+Pi}I^M$	2	ADP, Pi	Model	100 ns	2
$K^2N^{ADP}I^M$	2	ADP	Model	100 ns	2
$K^2N^-I^M$	2	–	Model	100 ns	2
$K^2N^{ATP}I^C$	2	ATP	Crystal	100 ns	2
$K^0N^{ATP}I^{R357}$	0	ATP	Model[a]	100 ns	1

[a]The side chain of R357 was oriented toward the γ-phosphate of ATP.

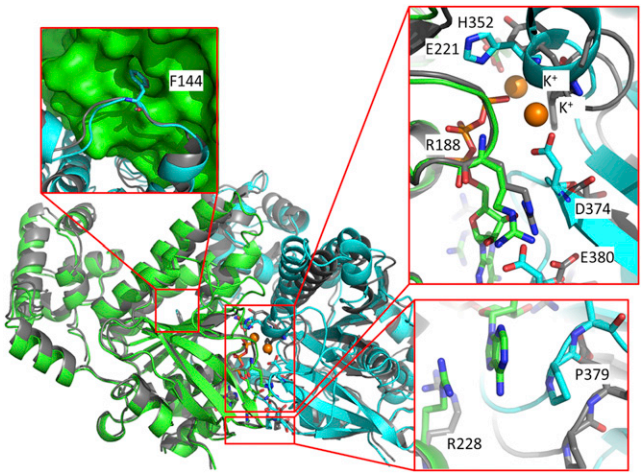

FIGURE 1 Homology modeling of yeast Rad51 dimer. The modeled structure (*green* (protomer A); *cyan* (protomer B)) was superimposed onto the crystal structure (*gray*). The binding mode of F144 in the polymerization motif is unchanged between the modeled and crystal structures (*upper left*). Protomer B pivots relative to protomer A, resulting in the movements of residues (H352, D374, P379, and E380) of protomer B at the ATP-binding site (*right*). In the modeled structure, the side chain of H352 in protomer B interacts with the ATP γ-phosphate, and the two K^+ mediate interactions between the ATP and D374 of protomer B and between ATP and the main chain of H352 (*upper right*). P379 of protomer B and R228 of protomer A sandwiched the adenine ring of ATP (*lower left*).

calculated using the Poisson-Boltzmann equation method implemented in CHARMM (26). The ion concentration in the Poisson-Boltzmann calculations was set at 100 mM. The protein and water dielectric constants were 1 and 80, respectively. For comparison, electrostatic energies of the P-loop containing ATPases and GTPases (RecA, RadA, Ras_RasGAP, and F_1 ATPase) were also calculated using the same procedure. The PDB structures of RecA, RadA, Ras_RasGAP, and F_1ATPase used were 3CMW, 1XU4, 1WQ1, and 2JDI, respectively. To evaluate the effects of positive charges supplied by the arginine and lysine fingers of adjacent protomers in RecA, Ras_RasGAP, and F_1ATPase, electrostatic energies of arginine or lysine mutants to alanine were compared with those of their wild-types. The mutant structures were generated by simply removing side chains beyond Cβ. In RadA, electrostatic energies of structures in which one or two bound K^+ ions removed were compared with those of the original crystal structure.

RESULTS

Homology modeling of yeast Rad51 dimer

An active dimer model of yeast Rad51 was constructed with homology modeling techniques combining a monomeric structure extracted from the crystal structure of yeast Rad51 (PDB ID: 3LDA) and the relative arrangement of a dimeric structure from the archaeal RadA crystal filament in the active form (PDB ID: 1XU4) (Fig. 1). Because each protomer of the target yeast Rad51 dimer has the same sequence as the reference yeast Rad51 crystal structure, except for the missing L1 and L2 loops and H352 mutations in the crystal structure, the modeled protomer structures closely resemble the Rad51 crystal structure. Cα-root mean-square deviations (RMSDs) between the modeled protomer and crystal structure were 0.67 ± 0.16 Å. In contrast, the relative arrangements of two protomers in the modeled dimer structures were more similar to that of the RadA crystal structure than the Rad51 crystal structure, because the dimer of the RadA crystal structure was used as one of the template structures, and in the monomeric Rad51 crystal structure used as another template, there was no information on the relative arrangement of two protomers in the dimer. Cα-RMSDs of the core domain in the modeled dimer to the corresponding part of the RadA crystal structure were 0.97 ± 0.01 Å, whereas those to the Rad51 crystal structure were 1.52 ± 0.03 Å.

Because no nucleotide is bound to the crystal structure of yeast Rad51, the ATP-binding site of Rad51 was modeled with reference to that of RadA. The protomer in which ATP is bound to the P-loop motif is referred to as protomer A, and the other protomer is referred to as protomer B. Although the original crystal structure of yeast Rad51 is more extended than the active form observed in EM studies, the helical pitch of the modeled structure is ~109 Å corresponding to the helical pitch of the active form. The binding mode of the polymerization motif (e.g., F144), which is a hot spot of interactions between adjacent protomers (27) is unchanged between the original crystal and modeled structures (Fig. 1). In the modeled structure, protomer B pivots about the polymerization motif relative to protomer A in contrast to the original crystal structure. Accordingly, the binding sites of the γ-phosphate (e.g., H352 and D374) and the adenine ring (e.g., P379) are spatially shifted from the crystal structure (Fig. 1).

In the crystal structures of RadA, one or two potassium ions are found at the binding site of the γ-phosphate of ATP (5,6). In the modeled structure of Rad51, we placed one or two potassium ions at the same positions as those of RadA (Fig. 1). Next, we performed multiple MD simulations with and without the potassium ions to examine how the potassium ions stabilize the dimer structure of Rad51 (Table 1).

Potassium ions stabilize Rad51 dimer

Throughout the MD simulations, individual domains, i.e., the N-terminal and core domains, of the Rad51 dimer were stable (Fig. S3). In contrast, the relative arrangements of the two protomers in the dimer exhibited significant variation depending on simulation conditions. The RMSDs of the two core domains in the dimer structure from the initial model are plotted in Fig. 2. In the simulations containing two K^+ ions (simulation $K^2N^{ATP}I^M$ in Table 1) and one K^+ ion (simulation $K^1N^{ATP}I^M$), the relative arrangements of the two protomers were stable during the simulations. In simulation $K^2N^{ATP}I^M$, an interaction network involving two K^+ ions was retained throughout the simulation (Fig. 3 *A*). Specifically, two K^+ ions mediated the interactions of the γ-phosphate with the backbone of H352 and

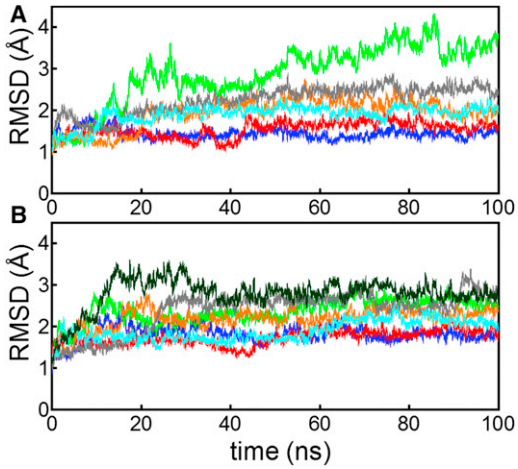

FIGURE 2 RMSD of the core domains of the Rad51 dimer from the initial structures in the first run (*panel A*) and second run (*panel B*) of simulations $K^2N^{ATP}I^M$ (*blue*), $K^1N^{ATP}I^M$ (*red*), $K^0N^{ATP}I^M$ (*green*), $K^2N^{ADP+Pi}I^M$ (*cyan*), $K^2N^{ADP}I^M$ (*orange*), and K^2NI^M (*gray*). The dark green line in panel *B* indicates the third run of $K^0N^{ATP}I^M$. In simulations containing K^+ ions, core domains were stable. In contrast, the K^+-free simulations exhibited large deviations from the modeled structure.

with the side chain of D374, and the side chain of H352 formed a direct or water-mediated hydrogen bond to the γ-phosphate (Figs. 3 *A* and 4 *A*). Thus, in Rad51, two K^+ ions and the phosphate of ATP functions as glue between adjacent protomers through interactions with the P-loop of protomer A and two residues, H352 and D374, of protomer B. In simulation $K^1N^{ATP}I^M$, because one of the K^+ ions was missing, the K^+-mediated interaction involving the γ-phosphate became weak. Therefore, the protomer interface in the vicinity of the γ-phosphate became open, as indicated by the distance between the Cα atoms of D374 in protomer B and K191 (the central residue of the P-loop motif) in protomer A (Figs. 3 *B* and 4 *B*). In contrast, the K^+-unbound simulation, $K^0N^{ATP}I^M$, showed that the binding site of the γ-phosphate became substantially open (Fig. 3 *C*). The relative arrangement of the two protomers also changed significantly (Fig. 2), whereas the binding at the polymerization motif was rigidly retained (Fig. 4 *C*). This large displacement was probably a result of the absence of mediation by K^+ ions for the interaction between the phosphate and D374. In simulation $K^0N^{ATP}I^M$, D374 formed a new salt bridge with R188 (the fourth residue of the P-loop motif, GXXXXGKT/S) of protomer A (Fig. S4). Because R188 initially formed a salt bridge with E380, R188 switched an interaction partner from E380 to D374. The salt bridge between R188 and D374 is also found in the crystal structure of yeast Rad51, suggesting that the salt bridge is a stable configuration in the K^+-unbound state. Consequently, the simulations with and without K^+ ions indicate that K^+ ions lead to the stable interactions of the ATP phosphate with the adjacent protomer of Rad51.

As another factor that impacts on stabilization of ATP-Rad51 interactions, the side chain of R357 was examined. By simple alternation of the side chain rotamer, the charged moiety of R357 can occupy the K^+ location. To examine this possibility, we modified the rotamer of R357 so that the side chain was oriented toward the ATP γ-phosphate in the modeled structure (Fig. S5). We then carried out MD simulations of the modified model without bound K^+ ions. In the MD simulations, the opening motion at the ATP-phosphate binding site was observed in a similar manner to the K^+-free simulation $K^0N^{ATP}I^M$, and the side chain of R357 tended to return to the original configuration, possibly due to interactions with E182 (Fig. S5). These results also indicate crucial roles of K^+ ions in the stabilization of the active form of Rad51.

To complement the MD simulations, electrostatic energies were calculated for the modeled structures with and without the bound K^+ ions. Clearly, the bound K^+ ions stabilize the electrostatic energies. Compared with the K^+-unbound structure, the K^+ ions decrease ~250 kcal/mol of

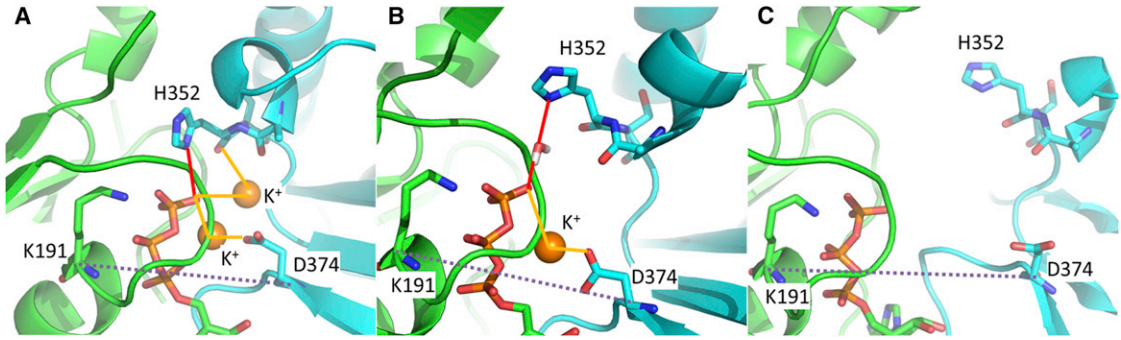

FIGURE 3 Effects of K^+ on the stability of the ATP-γ-phosphate binding site. The final structures of the ATP-γ-phosphate binding site in the first runs of simulations $K^2N^{ATP}I^M$ (*A*), $K^1N^{ATP}I^M$ (*B*), and $K^0N^{ATP}I^M$ (*C*) are shown. The dashed line indicates the distance between the Cα atoms of D374 and K191 that is used as an indicator of the opening of the interface. In panel *A*, a hydrogen bond between H352 and the γ-phosphate is shown with the red line, and interactions involving K^+ ions are shown in yellow lines. In simulations containing two K^+ ions, the ATP-binding site was tight. In the case of one K^+ ion, the side chain of H352 formed a water-mediated hydrogen bond with the γ-phosphate. In contrast, the K^+-free simulation exhibited a large opening motion at the ATP-binding site.

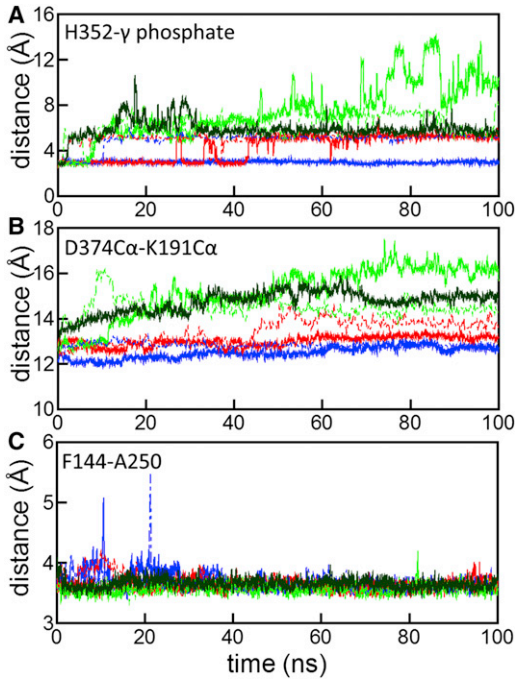

FIGURE 4 Effects of K^+ on the interactions between the two protomers of the dimer. In panel *A*, distances between the side chain of H352 and the γ-phosphate of ATP are shown. In panel *B*, distances between the Cα atoms of D374 and K191 are shown as an indicator of the opening of the dimer interface. In panel *C*, distances between the side chains of F144 and A250 in the polymerization-motif binding site are shown. The colors of the lines in all panels indicate simulations $K^2N^{ATP}I^M$ (*blue*), $K^1N^{ATP}I^M$ (*red*), and $K^0N^{ATP}I^M$ (*green*). Solid and dashed lines represent the results of the first and second runs, respectively. The third run of simulation $K^0N^{ATP}I^M$ is indicated by solid dark green lines.

electrostatic energies. In contrast, the modification of the R357 rotamer only slightly stabilizes the electrostatic energies. These results were consistent with the MD simulations. For comparison, we also calculated the electrostatic energies of other P-loop containing ATPases and GTPases. The details are described in the Discussion section.

Interestingly, E221, which is conserved among P-loop-containing ATPases and is supposed to play a role in activating a water molecule in ATP hydrolysis (28), occasionally formed a salt bridge with R308 in MD simulations (Fig. S6). Due to the salt bridge, the side chain of E221 was oriented away from the γ-phosphate of ATP. This interaction may cause the reduction of ATPase activity. In the RecA crystal structure, the arginine residue corresponding to R308 participates in interactions with the phosphate of the DNA backbone. Upon DNA binding, the salt bridge between E221 and R308 should be broken, and free E221 may increase ATPase activity. Thus, this salt bridge may be an explanation of low ATPase activity in the absence of DNA. However, to confirm the hypothesis, quantum mechanics/molecular mechanics studies for ATP hydrolysis and/or mutagenesis experiments should be performed.

Adenine ring of ATP also mediate dimer interactions

The adenine ring of ATP also mediates the interactions between adjacent protomers of Rad51. Both sides of the adenine ring are packed by R228 of protomer A and P379 of protomer B (Fig. 1). In all of the nucleotide-K^+-bound simulations starting from the modeled structure, the interactions of the adenine ring were stable throughout the simulations (Fig. 5, *A* and *B*). In contrast, in the nucleotide-free simulation $K^2N^-I^M$, the position of P379 of protomer B changed significantly (Fig. 5 *C* and Fig. S7), suggesting that interactions of the adenine ring are crucial for the relative arrangement of the two protomers in the active form of the Rad51. To confirm this result, an additional simulation ($K^2N^{ATP}I^C$) was conducted starting from the crystal structure of Rad51, in which P379 is shifted and apart from the adenine ring (Fig. 1). After ~40 ns in simulation $K^2N^{ATP}I^C$ (~10 ns in the second run), P379 was spontaneously in contact with the adenine ring of ATP (Fig. 5 *D* and Fig. S8). Consequently, our simulations suggest the interaction between P379 and the adenine ring contributes to the formation of the active filament of Rad51.

ATP hydrolysis destabilizes Rad51 dimer

Next, to investigate the effects of ATP hydrolysis on dimer stability, we conducted two MD simulations with ADP + Pi ($K^2N^{ADP+Pi}I^M$) and ADP ($K^2N^{ADP}I^M$). In the initial model of simulation $K^2N^{ADP+Pi}I^M$, which approximated the nucleotide state immediately after ATP hydrolysis, we replaced ATP with ADP and Pi; for this replacement, the quantum mechanics/molecular mechanics study of ATP hydrolysis in the F_1-ATPase that belongs to the same superfamily as Rad51 was consulted (28). For comparison, we performed an MD simulation including only ADP without Pi. The RMSD of the two core domains in simulations $K^2N^{ADP+Pi}I^M$ and $K^2N^{ADP}I^M$ were slightly larger than those of the ATP and K^+-bound simulations ($K^2N^{ATP}I^M$ and $K^1N^{ATP}I^M$) (Fig. 2), and the distances between D374 and K191 were larger than those of simulation $K^2N^{ATP}I^M$ (Figs. 4 *B* and 6 *A*). These findings indicate that the interprotomer interface at the γ-phosphate-binding site became open (Fig. 6 *B*). To characterize the opening motions in the ADP-bound simulations, we performed PCA for the trajectories of simulations $K^2N^{ATP}I^M$, $K^2N^{ADP+Pi}I^M$, and $K^2N^{ADP}I^M$. Because the core domain of protomer A was used for the structural alignment and the core domain of protomer B was used for calculation of the covariance matrix as described in the Methods, the principal modes in this analysis represent major motions of protomer B relative to protomer A. In this PCA, we do not intend to extract breathing motions during the simulations but to characterize the opening motions in $K^2N^{ADP+Pi}I^M$ and $K^2N^{ADP}I^M$.

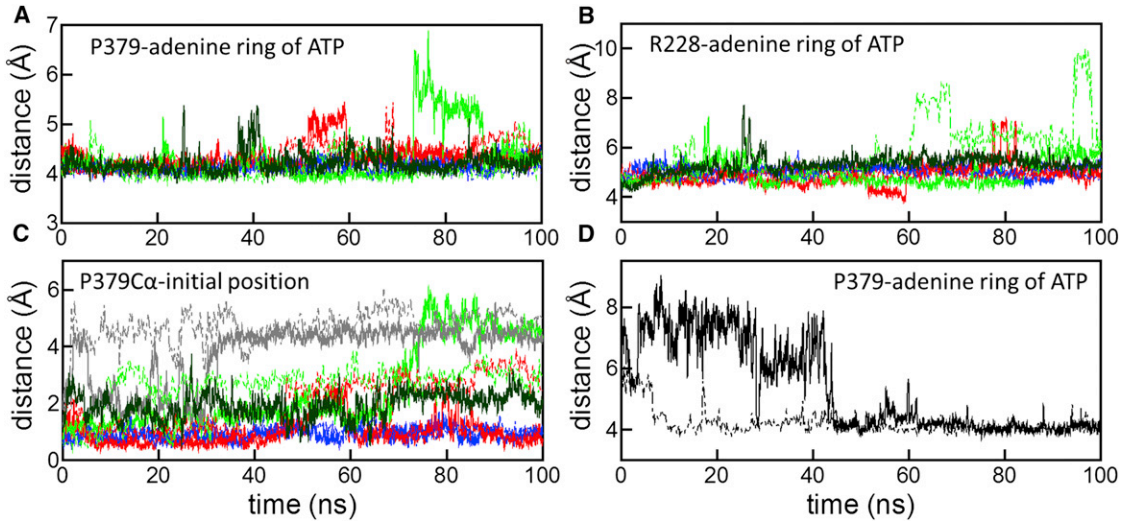

FIGURE 5 The adenine ring of ATP mediates interactions between adjacent protomers. In panel *A*, distances between the centers of mass of the P379 side chain (protomer B) and of the adenine ring of ATP are shown. In panel *B*, distances between the centers of mass of the R228 side chain (protomer A) and of the adenine ring of ATP are shown. In panel *C*, displacements of the Cα of P379 (protomer B) from the initial position during simulations are shown. In panels *A–C*, the colors of the lines indicate simulations $K^2N^{ATP}I^M$ (*blue*), $K^1N^{ATP}I^M$ (*red*), $K^0N^{ATP}I^M$ (*green*), and $K^2N^-I^M$ (*gray*). In panel *D*, in simulation $K^2N^{ATP}I^C$ starting from the crystal structure, distances between the centers of mass of the P379 side chain (protomer B) and of the adenine ring of ATP are shown. The spontaneous binding of P379 to the adenine ring was observed. Solid and dashed lines represent the results of the first and second runs, respectively. The third run of simulation $K^0N^{ATP}I^M$ is indicated by solid dark green lines.

Fig. 7 *A* shows that the first principal component (PC1) representing the largest motions discriminates the post-hydrolysis trajectories ($K^2N^{ADP+Pi}I^M$ and $K^2N^{ADP}I^M$) from the prehydrolysis trajectory ($K^2N^{ATP}I^M$). Structural transitions in posthydrolysis trajectories took place during the first 10–20 ns. The cosine contents of PC1 of trajectories $K^2N^{ADP+Pi}I^M$ (9%) and $K^2N^{ADP}I^M$ (41%) in the first run are not very high, indicating that the motions of posthydrolysis trajectories are different from the random diffusion on a flat potential surface. However, the directions of PC1 and PC2 in the second run were swapped in comparison to the directions in the first run (Fig. S9), suggesting that the opening motions are stochastic rather than deterministic. The directions of PC1 and PC2 are depicted in Fig. 7 *C*. To visualize the PC1 and PC2 motions of the Rad51 protomer in the Rad51-dsDNA filament, the filament model was constructed by superimposing the average dimer structure onto the crystal structure of the RecA-dsDNA complex and replacing RecA protomers with Rad51 protomers. The directions of the PC modes appear to correspond to dissociation directions of a terminal Rad51 protomer from DNA. Because the phosphate of the bound ATP is oriented toward the DNA (see Fig. 7 *C*), the opening motion at the ATP-phosphate binding site may initiate dissociation of a terminal protomer from the nucleoprotein filament. This observation is consistent with single-molecule experiments in which Rad51 protomers dissociate from the terminus of the filament after ATP hydrolysis (29). However, because our simulations did not include DNA, effects of ATP hydrolysis on Rad51-DNA binding should be investigated using simulations of the Rad51-DNA complex in the future.

DISCUSSION

Our simulation results indicated that one or two K^+ ions stabilize the Rad51 active form and are consistent with experimental data. Although Rad51 exhibits weak strand exchange activity compared with RecA in vitro, salts can stimulate the strand exchange activity of human Rad51 (30). This strand exchange stimulation in human Rad51 is dependent on the cation component of salts. The NH_4^+ or K^+ cations can stimulate the strand exchange, whereas the Na^+ cation is incapable of stimulating the strand exchange. In a recent EM study, the human Rad51 filament exhibits the relatively short helical pitch of ~86 Å without salts. In contrast, by adding salts containing the NH_4^+ or K^+ cation, the helical pitch is extended to ~110 Å, which corresponds to the active form, suggesting that the cations stabilize the active form of human Rad51 (31). Yeast Rad51 also exhibits a requirement of KCl in its strand exchange reaction (32). In addition to monovalent cations, the divalent Ca^{2+} cation also stimulates the strand exchange reaction of human Rad51 (33) by stabilizing the active form of the human Rad51 filament (34). However, Ca^{2+} does not stimulate the strand exchange activity of yeast Rad51, although most of the residues in the ATP-binding site are conserved between the two species.

The ATPase activity is also affected by the cation component. In archaeal recombinase RadA, DNA-stimulated

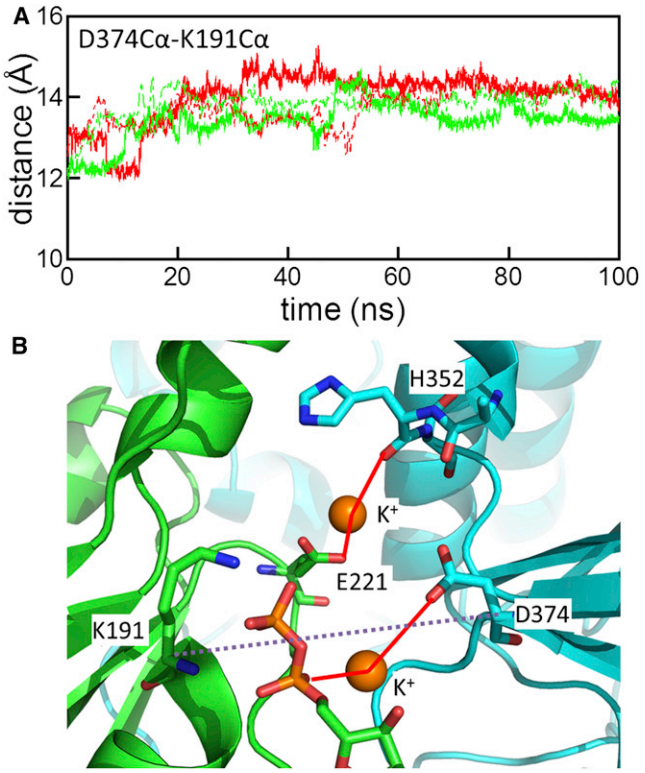

FIGURE 6 Opening of the dimer interface in ADP-bound simulations. In panel *A*, distances between the Cα atoms of D374 and K191 in simulations $K^2N^{ADP+Pi}I^M$ (*green*) and $K^2N^{ADP}I^M$ (*red*) are shown. Solid and dashed lines represent the results of the first and second runs, respectively. In panel *B*, the ATP-binding site of the final structure in simulation $K^2N^{ADP}I^M$ of the first run is shown. Red lines indicate interactions involving K^+ ions. The dashed line is drawn to indicate the distance between D374 and K191.

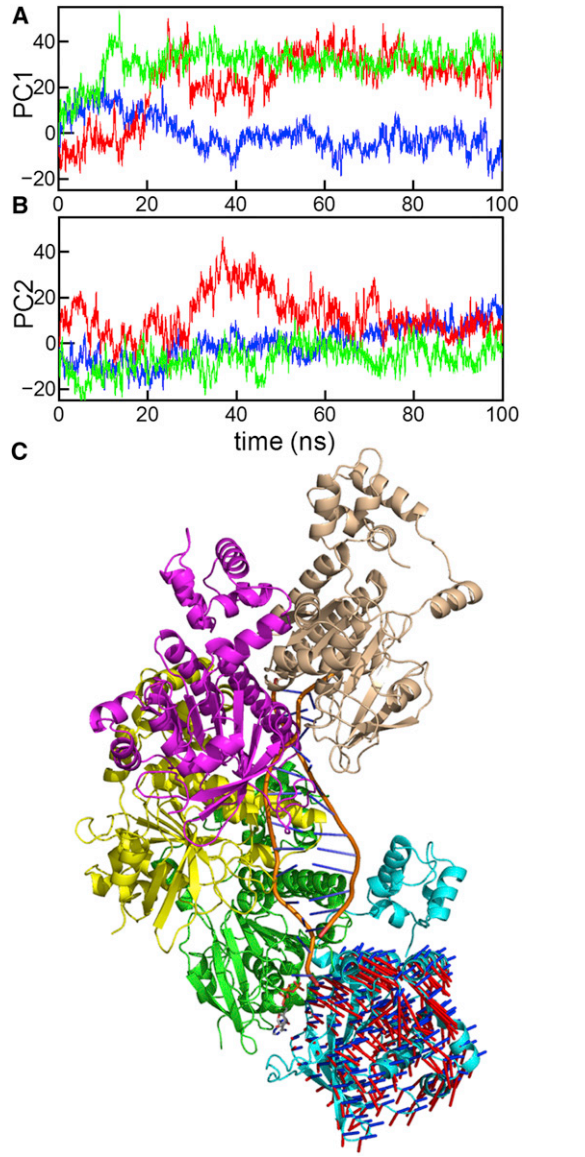

FIGURE 7 PCA for trajectories of the ADP-bound simulations. Projections of snapshots onto PC1 and PC2 in the first run of simulations $K^2N^{ATP}I^M$ (*blue*), $K^2N^{ADP+Pi}I^M$ (*green*), and $K^2N^{ADP}I^M$ (*red*) are shown in panels *A* and *B*, respectively. PC1 discriminates the posthydrolysis trajectories ($K^2N^{ADP+Pi}I^M$ and $K^2N^{ADP}I^M$) from the prehydrolysis trajectory ($K^2N^{ATP}I^M$). The cosine contents of PC1 in $K^2N^{ATP}I^M$, $K^2N^{ADP+Pi}I^M$, and $K^2N^{ADP}I^M$ are 34%, 9%, and 41%, respectively. The cosine contents of PC2 in $K^2N^{ATP}I^M$, $K^2N^{ADP+Pi}I^M$, and $K^2N^{ADP}I^M$ are 0.2%, 6%, and 28%, respectively. In panel *C*, the directions of PC1 (*red lines*) and PC2 (*blue lines*) are shown in the Rad51-dsDNA filament (3 × square root of eigen values). The filament model was constructed by superimposing the average dimer structure onto the crystal structure of the RecA-dsDNA complex and replacing RecA protomers with Rad51 protomers. The bound ATP in the dimer was shown in stick representation.

ATPase activity requires the K^+ cation (5). No ATPase activity was observed in the presence of salts containing the Na^+ cation. However, human Rad51 exhibits the ATPase activity even in the presence of NaCl (30). It should be noted that the increase in ATPase activity does not always enhance the strand exchange activity. For instance, Ca^{2+} reduces the ATPase activity of human Rad51 but enhances the strand exchange activity (33). Ca^{2+} appears to maintain the active form of the Rad51 filament by reducing the ATP hydrolysis rate.

DNA binding also affects the ATPase activity of Rad51 and RadA (5,30). Although our simulation did not include DNA, our simulation results suggest possible linkages between the DNA- and ATP-binding sites. In our simulations, K^+ ions stabilized interactions between the γ-phosphate of ATP and the H352-containing α-helix in the downstream region of the L2 loop that is crucial for DNA binding. In the RadA crystal structures with low K^+ concentrations or in the presence of ADP instead of AMP-PNP, the corresponding α-helix is disordered (6). By stabilizing the L2 loop and the downstream α-helix, DNA binding may affect the ATPase activity of Rad51. In addition, our simulation suggests that R308 could potentially regulate ATP activity by the salt bridge with E221 that activates a water molecule in ATP hydrolysis as described in the Results section.

In vivo, in addition to cations, other factors such as mediators have effects on Rad51 strand exchange activity. For

instance, the protein complex, Swi5-Sfr1, which is conserved from fission yeast to human, stabilizes the active form of fission yeast Rad51 and enhances the ATPase activity of Rad51 (35–37).

In our simulations, one of the K^+ ions mediated interactions between the γ-phosphate of ATP and D374, belong to the adjacent protomer. The other K^+ ion interacted with both the ATP γ-phosphate and the H352 backbone of the adjacent protomer. Recognition of the ATP phosphate by the adjacent protomer is a common feature among P-loop-containing ATPases and GTPases (Fig. S1). In the bacterial recombinase RecA, two lysine side chains of the adjacent protomer recognize the phosphate of ATP (Fig. 8) (9). Similarly, in ATP synthase, an arginine side chain of an adjacent subunit directly interacts with the phosphate of ATP (10). In Rasp21, which functions in signal transduction, an arginine side chain of a binding partner, GTPase-activating protein (GAP), binds to the phosphate of ATP (11). Thus, recognition of the nucleotide phosphate by a moiety of an adjacent protomer is shared among these P-loop containing ATPases and GTPases. In the case of Rad51 as well as RadA, two K^+ ions, H352 and D374 play roles in recognition of the nucleotide phosphate. To confirm stabilization of ATP-protein interactions by supplying positive charges, we counted the number of charged residues of these P-loop containing ATPases in the vicinity of the ATP phosphate. Even including the supplied positive charges of adjacent protomers and cations, the net charge in the vicinity of the ATP phosphate is slightly negative, suggesting that the supplied positive charges contribute to stabilizing ATP-protein interactions (Table S2). Electrostatic energies calculated using the Poisson-Boltzmann equation also clearly indicate that the supplied positive charges stabilized the complex structure (Fig. 9), consistent with our MD simulations. Interestingly, in paralogs of human Rad51, D316, which corresponds to D374 of yeast Rad51, is mutated to lysine (31). EM of the human Rad51 D316K mutant showed that even without salts, the helical pitch is ~110 Å, corresponding to the active form. In the crystal structure of the RadA D302K mutant, in which D302 corresponds to D374 of yeast Rad51 and D316 of human Rad510, K302 directly interacts with the ATP γ-phosphate. These experimental results are clearly consistent with our simulation results.

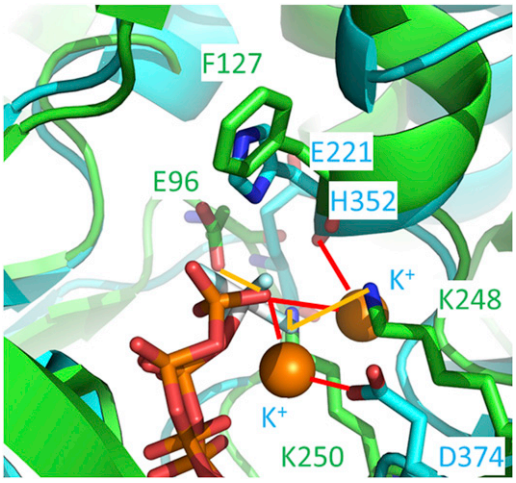

FIGURE 8 Comparison between the ATP-binding sites of the final structure of the $K^2N^{ATP}I^M$ simulation (*cyan*) and RecA (PDB code 3CMW, *green*). The K^+ ions (*orange spheres*) in the simulation structure and the lysine side chains of RecA are located in similar positions.

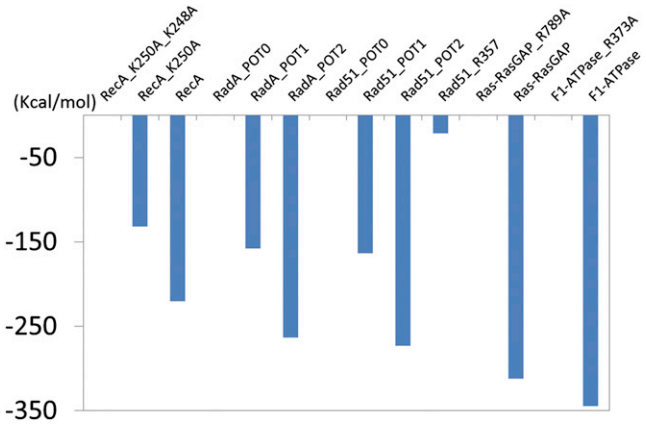

FIGURE 9 Electrostatic energies of P-loop containing ATPases and GTPases decreased due to positive charges supplied by the arginine and lysine fingers of adjacent protomers and K^+ ions. Relative energies to those without the supplied positive charges are shown. Electrostatic energies were calculated using the Poisson-Boltzmann equation. In RecA, Ras_RasGAP, and F_1ATPase, mutants of lysine and arginine fingers were compared with their wild-types. In RadA and Rad51, structures with one or two K^+ ions in the ATP-binding site were compared with those in the absence of bound K^+ ions. Rad51 with the modified configuration of R357 in the absence of the K^+ ion was also compared.

Very recently, molecular modeling and MD simulations of human Rad51 were reported (34). This work focused on Ca^{2+} and Mg^{2+} ions rather than the K^+ ions we studied for this work. The researchers found that when a Ca^{2+} or Mg^{2+} ion was missing from the vicinity of the γ-phosphate of ATP, local structures close to the γ-phosphate became unstable. Considering that the charge of a Ca^{2+} ion is the same as that of two K^+ ions, their results are in good agreement with our results. However, Ca^{2+} does not stimulate the strand exchange activity of yeast Rad51 in contrast to human Rad51 (33), as described previously. Interestingly, in RadA, a crystal structure in which one Ca^{2+} ion is bound to the same position as two K^+ ions has been reported (7).

In summary, we constructed a dimer model of Rad51 in the active form of the filament using homology modeling techniques, and performed MD simulations from the modeled structures with explicit solvent. We found two crucial interaction networks involving ATP: one is an interaction network among the γ-phosphate of ATP, K^+ ions, H352, and D374; the other is among the adenine ring of ATP, R228, and P379. We also investigated how ATP hydrolysis affects the connection of the two protomers in the

active form of Rad51. In the MD simulation starting from a structure mimicking the state immediately after ATP hydrolysis, the interaction network involving the phosphate of ATP was significantly perturbed, resulting in an opening motion at the dimer interface. This opening motion occurred in the direction in which the terminal protomer dissociated from DNA. These results support that one of the functional roles of ATP γ-phosphate and K^+ is as glue between the protomers in the active form of Rad51.

SUPPORTING MATERIAL

Two supporting tables, nine figures, and a PDB file are available at http://www.biophysj.org/biophysj/supplemental/S0006-3495(13)00204-X.

We thank Hiroshi Iwasaki for helpful discussions.

This study was supported by Grants-in-Aids for Scientific Research on Innovative Areas from the Ministry of Education, Culture, Sports, Science, and Technology of Japan (MEXT) and for Scientific Research (B); by the Grand Challenges in Next-Generation Integrated Simulation of Living Matter, which is part of the Development and Use of the Next-Generation Supercomputer Project of MEXT; by Platform for Drug Design, Informatics and Structural Life Sciences (MEXT); by X-ray Free Electron Laser Priority Strategy Program (MEXT).

REFERENCES

1. Bianco, P. R., R. B. Tracy, and S. C. Kowalczykowski. 1998. DNA strand exchange proteins: a biochemical and physical comparison. *Front. Biosci.* 3:D570–D603.
2. Brendel, V., L. Brocchieri, …, S. Karlin. 1997. Evolutionary comparisons of RecA-like proteins across all major kingdoms of living organisms. *J. Mol. Evol.* 44:528–541.
3. Story, R. M., I. T. Weber, and T. A. Steitz. 1992. The structure of the *E. coli recA* protein monomer and polymer. *Nature.* 355:318–325.
4. Bell, C. E. 2005. Structure and mechanism of *Escherichia coli* RecA ATPase. *Mol. Microbiol.* 58:358–366.
5. Wu, Y., X. Qian, …, Y. Luo. 2005. Crystal structure of an ATPase-active form of Rad51 homolog from *Methanococcus voltae*. Insights into potassium dependence. *J. Biol. Chem.* 280:722–728.
6. Qian, X., Y. Wu, …, Y. Luo. 2005. Crystal structure of *Methanococcus voltae* RadA in complex with ADP: hydrolysis-induced conformational change. *Biochemistry.* 44:13753–13761.
7. Qian, X., Y. He, …, Y. Luo. 2006. Calcium stiffens archaeal Rad51 recombinase from *Methanococcus voltae* for homologous recombination. *J. Biol. Chem.* 281:39380–39387.
8. VanLoock, M. S., X. Yu, …, E. H. Egelman. 2003. ATP-mediated conformational changes in the RecA filament. *Structure.* 11:187–196.
9. Chen, Z., H. Yang, and N. P. Pavletich. 2008. Mechanism of homologous recombination from the RecA-ssDNA/dsDNA structures. *Nature.* 453:489–494.
10. Bowler, M. W., M. G. Montgomery, …, J. E. Walker. 2007. Ground state structure of F_1-ATPase from bovine heart mitochondria at 1.9 Å resolution. *J. Biol. Chem.* 282:14238–14242.
11. Scheffzek, K., M. R. Ahmadian, …, A. Wittinghofer. 1997. The Ras-RasGAP complex: structural basis for GTPase activation and its loss in oncogenic Ras mutants. *Science.* 277:333–338.
12. Conway, A. B., T. W. Lynch, …, P. A. Rice. 2004. Crystal structure of a Rad51 filament. *Nat. Struct. Mol. Biol.* 11:791–796.
13. Chen, J., N. Villanueva, …, S. W. Morrical. 2010. Insights into the mechanism of Rad51 recombinase from the structure and properties of a filament interface mutant. *Nucleic Acids Res.* 38:4889–4906.
14. Reymer, A., K. Frykholm, …, B. Nordén. 2009. Structure of human Rad51 protein filament from molecular modeling and site-specific linear dichroism spectroscopy. *Proc. Natl. Acad. Sci. USA.* 106:13248–13253.
15. Altschul, S. F., T. L. Madden, …, D. J. Lipman. 1997. Gapped BLAST and PSI-BLAST: a new generation of protein database search programs. *Nucleic Acids Res.* 25:3389–3402.
16. Thompson, J. D., T. J. Gibson, …, D. G. Higgins. 1997. The CLUSTAL_X windows interface: flexible strategies for multiple sequence alignment aided by quality analysis tools. *Nucleic Acids Res.* 25:4876–4882.
17. Notredame, C., D. G. Higgins, and J. Heringa. 2000. T-Coffee: a novel method for fast and accurate multiple sequence alignment. *J. Mol. Biol.* 302:205–217.
18. Edgar, R. C. 2004. MUSCLE: multiple sequence alignment with high accuracy and high throughput. *Nucleic Acids Res.* 32:1792–1797.
19. Sali, A., and T. L. Blundell. 1993. Comparative protein modelling by satisfaction of spatial restraints. *J. Mol. Biol.* 234:779–815.
20. Laskowski, R. A., M. W. MacArthur, …, J. M. Thornton. 1993. PROCHECK: a program to check the stereochemical quality of protein structures. *J. Appl. Cryst.* 26:283–291.
21. Ikeguchi, M. 2004. Partial rigid-body dynamics in NPT, NPAT and NPgammaT ensembles for proteins and membranes. *J. Comput. Chem.* 25:529–541.
22. Mackerell, Jr., A. D., M. Feig, and C. L. Brooks, 3rd. 2004. Extending the treatment of backbone energetics in protein force fields: limitations of gas-phase quantum mechanics in reproducing protein conformational distributions in molecular dynamics simulations. *J. Comput. Chem.* 25:1400–1415.
23. MacKerell, Jr., A. D., N. Banavali, and N. Foloppe. 2000-2001. Development and current status of the CHARMM force field for nucleic acids. *Biopolymers.* 56:257–265.
24. Jorgensen, W. L., J. Chandrasekhar, …, M. L. Klein. 1983. Comparison of simple potential functions for simulating liquid water. *J. Chem. Phys.* 79:926–935.
25. Hess, B. 2000. Similarities between principal components of protein dynamics and random diffusion. *Phys. Rev. E Stat. Phys. Plasmas Fluids Relat. Interdiscip. Topics.* 62(6 Pt B):8438–8448.
26. Brooks, B. R., R. E. Bruccoleri, …, M. Karplus. 1983. CHARMM: a program for macromolecular energy, minimization, and dynamics calculations. *J. Comput. Chem.* 4:187–217.
27. Pellegrini, L., D. S. Yu, …, A. R. Venkitaraman. 2002. Insights into DNA recombination from the structure of a RAD51-BRCA2 complex. *Nature.* 420:287–293.
28. Hayashi, S., H. Ueno, …, H. Noji. 2012. Molecular mechanism of ATP hydrolysis in F_1-ATPase revealed by molecular simulations and single-molecule observations. *J. Am. Chem. Soc.* 134:8447–8454.
29. van Mameren, J., M. Modesti, …, G. J. Wuite. 2009. Counting RAD51 proteins disassembling from nucleoprotein filaments under tension. *Nature.* 457:745–748.
30. Shim, K. S., C. Schmutte, …, R. Fishel. 2006. Defining the salt effect on human RAD51 activities. *DNA Repair (Amst.).* 5:718–730.
31. Amunugama, R., Y. He, …, R. Fishel. 2012. RAD51 protein ATP cap regulates nucleoprotein filament stability. *J. Biol. Chem.* 287:8724–8736.
32. Rice, K. P., A. L. Eggler, …, M. M. Cox. 2001. DNA pairing and strand exchange by the *Escherichia coli* RecA and yeast Rad51 proteins without ATP hydrolysis: on the importance of not getting stuck. *J. Biol. Chem.* 276:38570–38581.
33. Bugreev, D. V., and A. V. Mazin. 2004. Ca^{2+} activates human homologous recombination protein Rad51 by modulating its ATPase activity. *Proc. Natl. Acad. Sci. USA.* 101:9988–9993.

34. Fornander, L. H., K. Frykholm, …, B. Nordén. 2012. Ca^{2+} improves organization of single-stranded DNA bases in human Rad51 filament, explaining stimulatory effect on gene recombination. *Nucleic Acids Res.* 40:4904–4913.

35. Haruta, N., Y. Akamatsu, …, H. Iwasaki. 2008. Fission yeast Swi5 protein, a novel DNA recombination mediator. *DNA Repair (Amst.).* 7:1–9.

36. Kokabu, Y., Y. Murayama, …, M. Ikeguchi. 2011. Fission yeast Swi5-Sfr1 protein complex, an activator of Rad51 recombinase, forms an extremely elongated dogleg-shaped structure. *J. Biol. Chem.* 286:43569–43576.

37. Kuwabara, N., Y. Murayama, …, T. Shimizu. 2012. Mechanistic insights into the activation of Rad51-mediated strand exchange from the structure of a recombination activator, the Swi5-Sfr1 complex. *Structure.* 20:440–449.

Supporting Information for

Molecular Modeling and Molecular Dynamics Simulations of Recombinase Rad51

Yuichi Kokabu[a] and Mitsunori Ikeguchi[a]

[a]Graduate School of Nanobioscience, Yokohama City University, 1-7-29 Suehiro-cho, Tsurumi-ku, Yokohama, 230-0045, Japan.

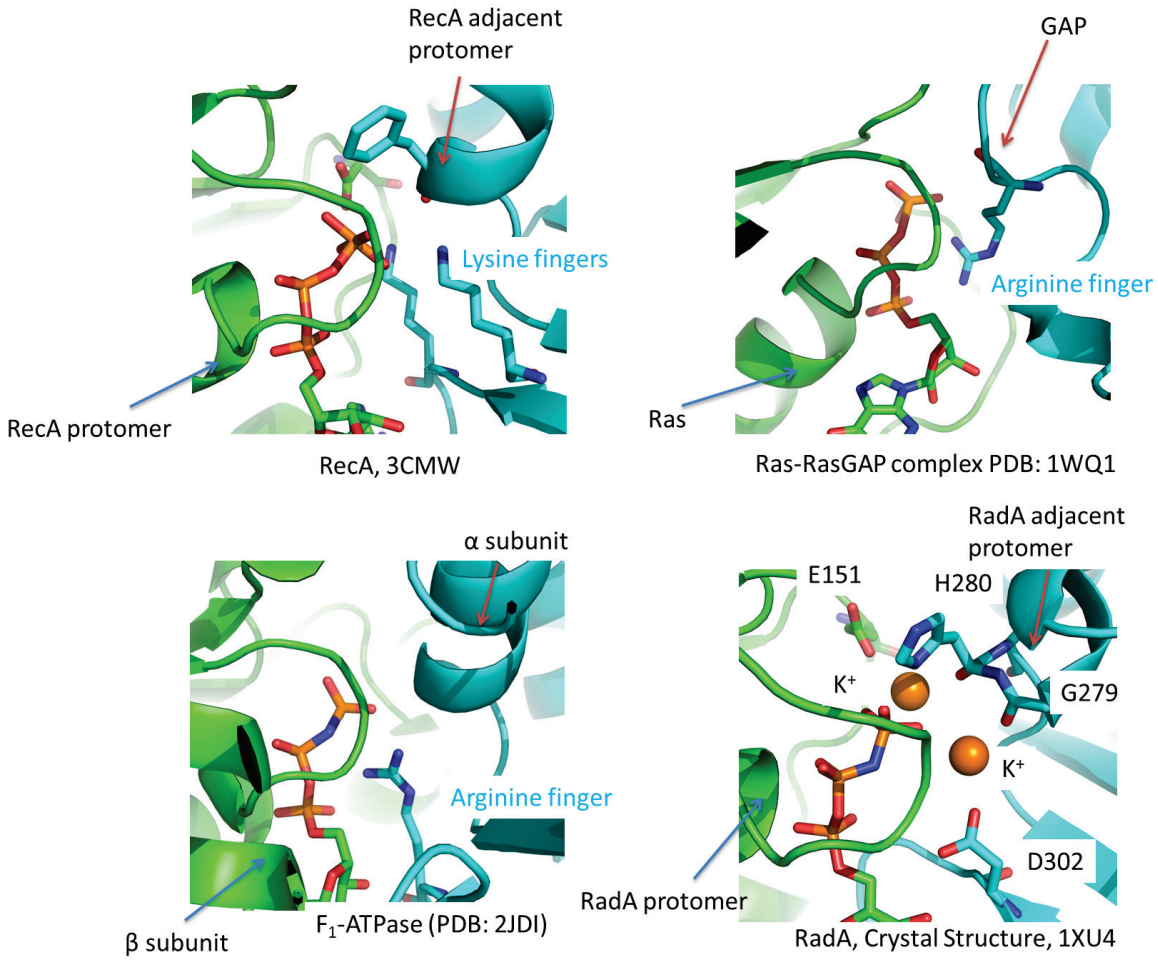

Figure S1. Recognitions of ATP and GTP phosphates in P-loop-containing ATPases and GTPases. Two lysine fingers in the RecA adjacent protomer recognized the ATP phosphate in the crystal structure (PDB code 3CMW; upper left). In the Ras-RasGAP complex that functions in the signal transduction, an arginine finger of RasGAP interacts with the GTP phosphate (PDB code 1WQ1; upper right). In ATP synthase, an arginine finger of the non-catalytic α subunit interacts with the ATP bound in the catalytic β subunit (PDB code 2JDI; lower left). In archaeal RadA, two K^+ ions interact with ATP in a similar manner to other lysine and arginine fingers (PDB code 1XU4; lower right).

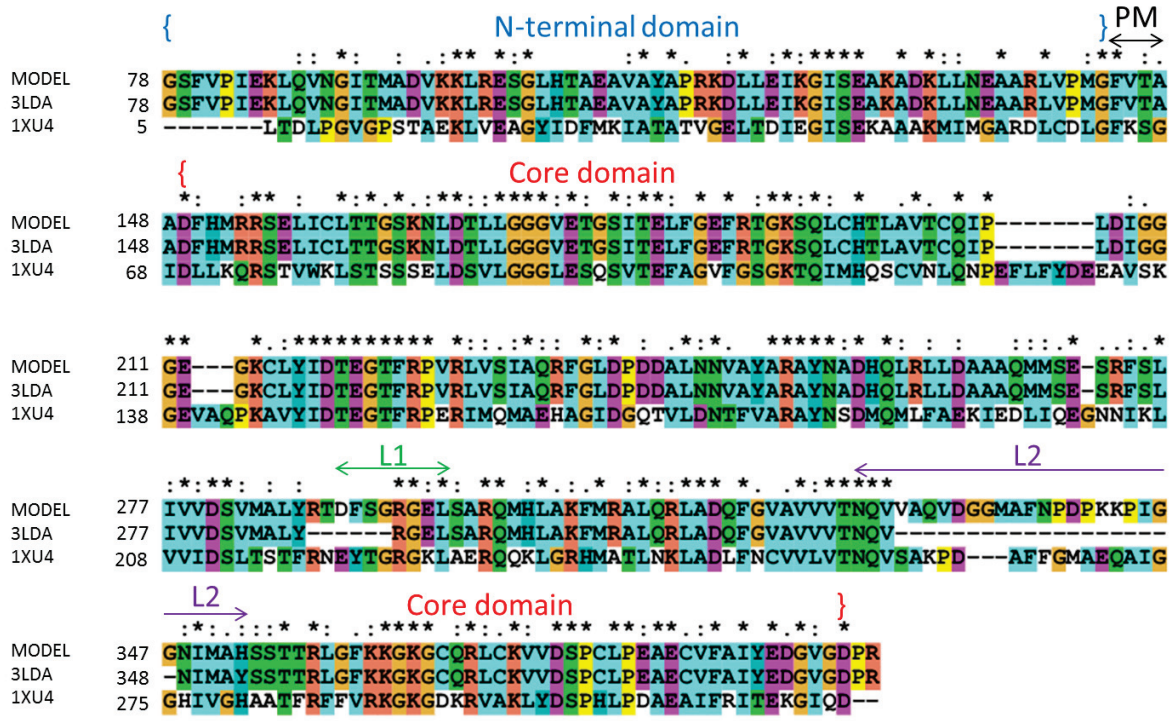

Figure S2. Blast alignment used to generate the model. The sequence alignment of the modeled structure (MODEL) and the crystal structures of Yeast Rad51 (3LDA) and RadA (1XU4) is shown. The sequences of the modeled structure and 3LDA are the same except for L1, L2 and His352. His352 is mutated to Tyr in 3LDA.

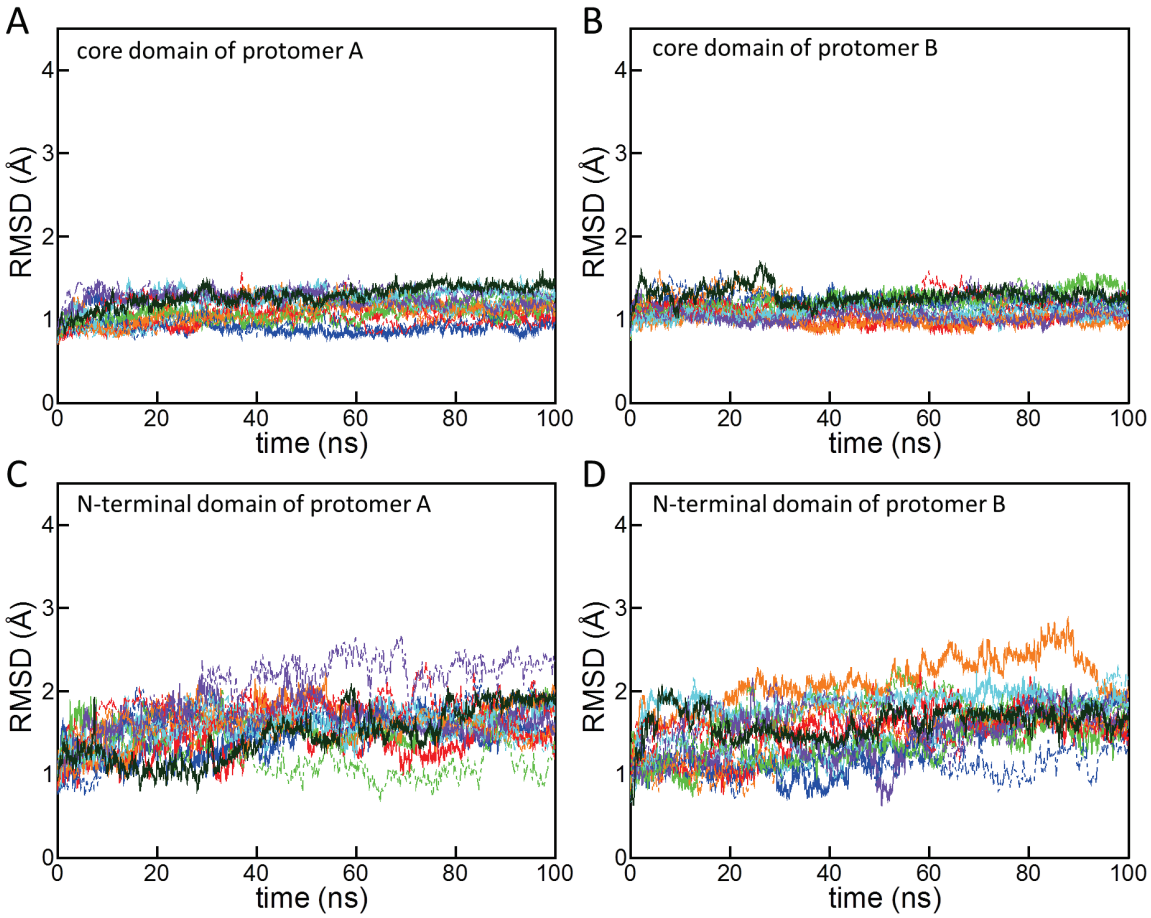

Figure S3. RMSD of each domain during MD simulations from initial structures. In panels *A, B*, *C*, and *D,* the RMSDs of the core domain of protomer A, the core domain of protomer B, the N-terminal domain of protomer A (residues 78-139), and N-terminal domain of protomer B are shown, respectively. The colors of the lines indicate simulations $K^2N^{ATP}I^M$ (blue), $K^1N^{ATP}I^M$ (red), $K^0N^{ATP}I^M$ (green), $K^2N^{ADP+Pi}I^M$ (cyan), $K^2N^{ADP}I^M$ (orange), $K^2N^{-}I^M$ (purple), and the third run of $K^0N^{ATP}I^M$ (dark green). Solid and dashed lines represent the results of the first and second runs, respectively.

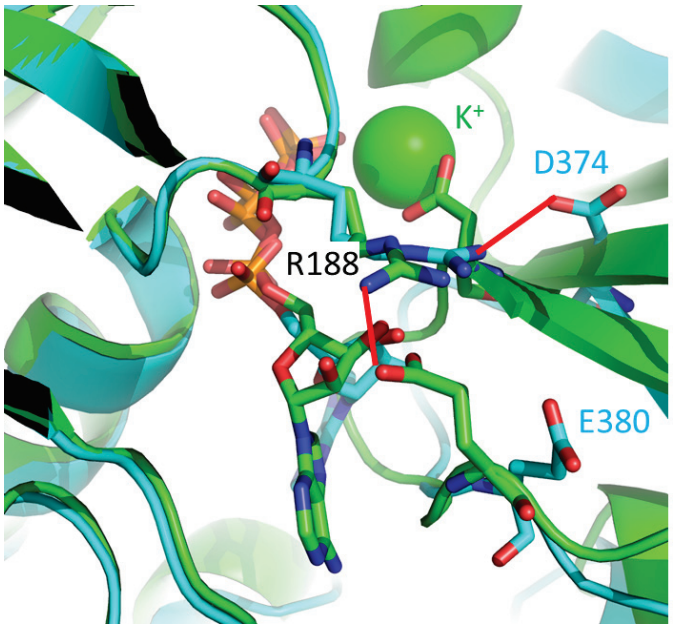

Figure S4. Switching of an R188 interaction partner from E380 to D374. In the initial model structure (green), R188 formed a salt bridge with E380. In the final structure of simulation $K^{0}N^{ATP}I^{M}$ (cyan), R188 changed its interaction partner to D374.

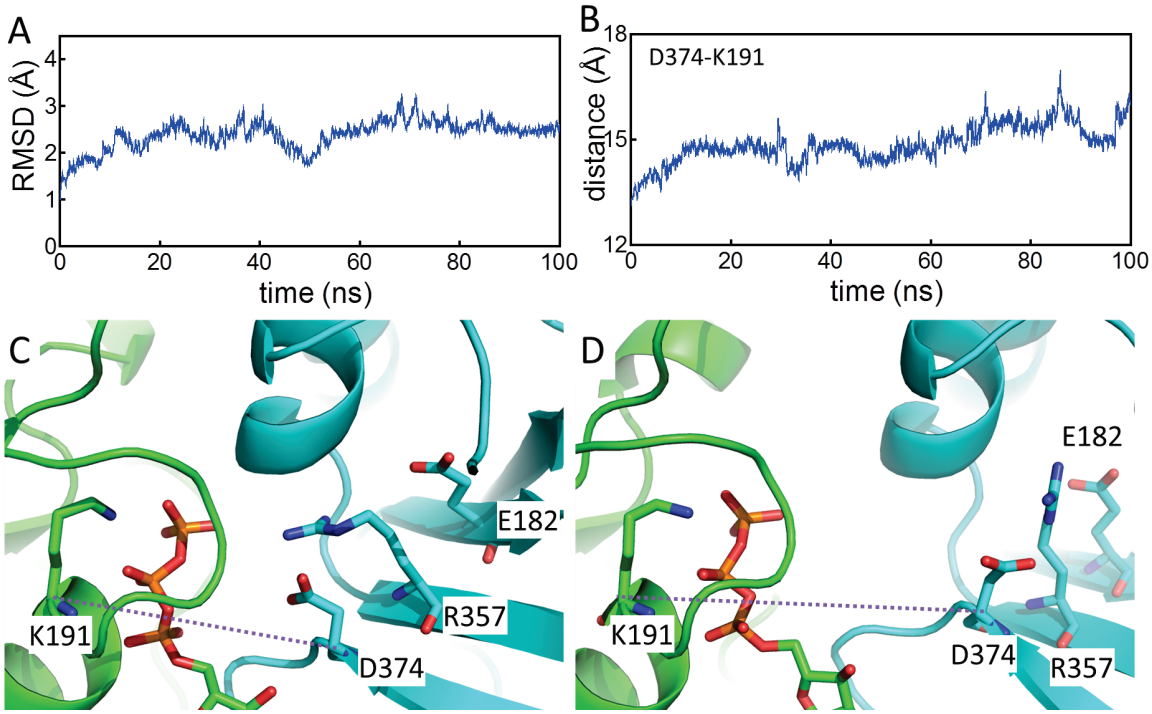

Figure S5. MD simulation from the modeled structure, in which the side chain of R357 is oriented toward the ATP γ-phosphate. In panel *A*, the RMSD of the core domains of the Rad51 dimer from the initial structure is plotted against the simulation time. In panel *B*, distances between the Cα atoms of D374-K191 are shown. Rad51 undergoes an opening motion at the ATP binding site. In panel *C*, the ATP binding site of the modified initial model is shown. The R357 side chain is oriented toward the ATP γ phosphate. In panel *D*, the ATP binding site of the final structure of the simulation is shown. The side chain of R357 returned to the original configuration and interacted with E182. The dashed line indicates the distance between the Cα atoms of D374 and K191.

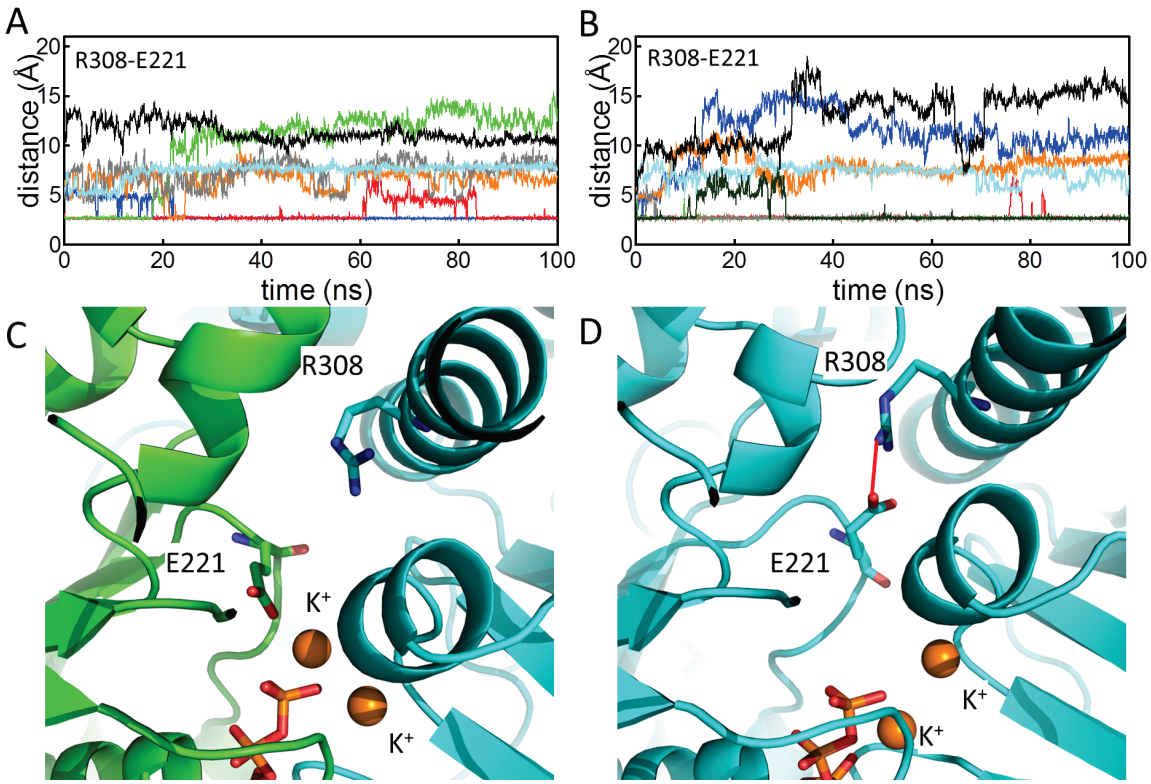

Figure S6. The salt bridge between E221 and R308. In panels *A* and *B*, distances between R308 and E221 in the first and second runs are shown, respectively. The colors of the lines indicate the $K^2N^{ATP}I^M$ (blue), $K^1N^{ATP}I^M$ (red), $K^0N^{ATP}I^M$ (green), $K^2N^{ADP+Pi}I^M$ (cyan), $K^2N^{ADP}I^M$ (orange), $K^2N^-I^M$ (gray), and $K^2N^{ATP}I^C$ (black) simulations and the third run of $K^0N^{ATP}I^M$ (dark green). In panel *C*, the ATP-phosphate binding site in the initial model is shown. E221 is oriented toward the ATP γ-phosphate. In panel *D*, the final structure of simulation $K^2N^{ATP}I^M$ is shown. E221, which forms a salt bridge with R308, is oriented away from the ATP γ-phosphate.

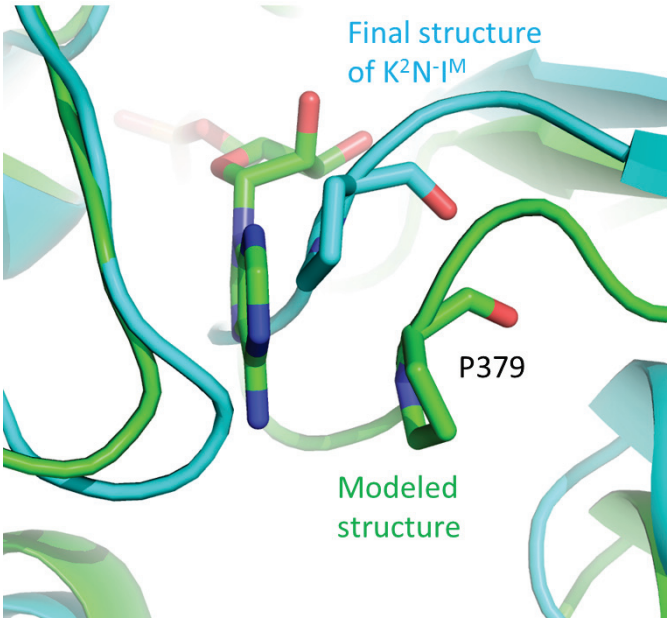

Figure S7. Movements of P379 in the nucleotide-free simulation $K^2N^-I^M$. The location of P379 changed significantly from the initial model (green) to the final structure of simulation $K^2N^-I^M$ (cyan).

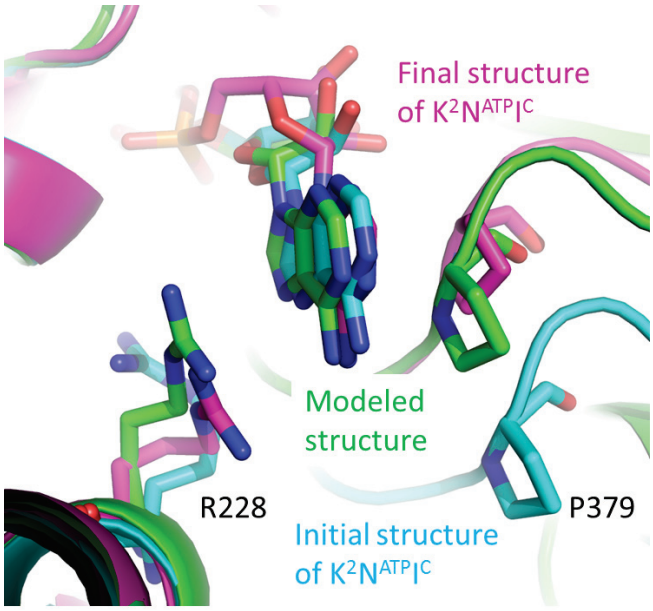

Figure S8. Spontaneous formation of interaction between the adenine ring of ATP and P379 in the $K^2N^{ATP}I^C$ simulation starting from the crystal structure (cyan). The P379 location in the final structure of the $K^2N^{ATP}I^C$ (magenta) simulation is similar to that of the modeled structure (green).

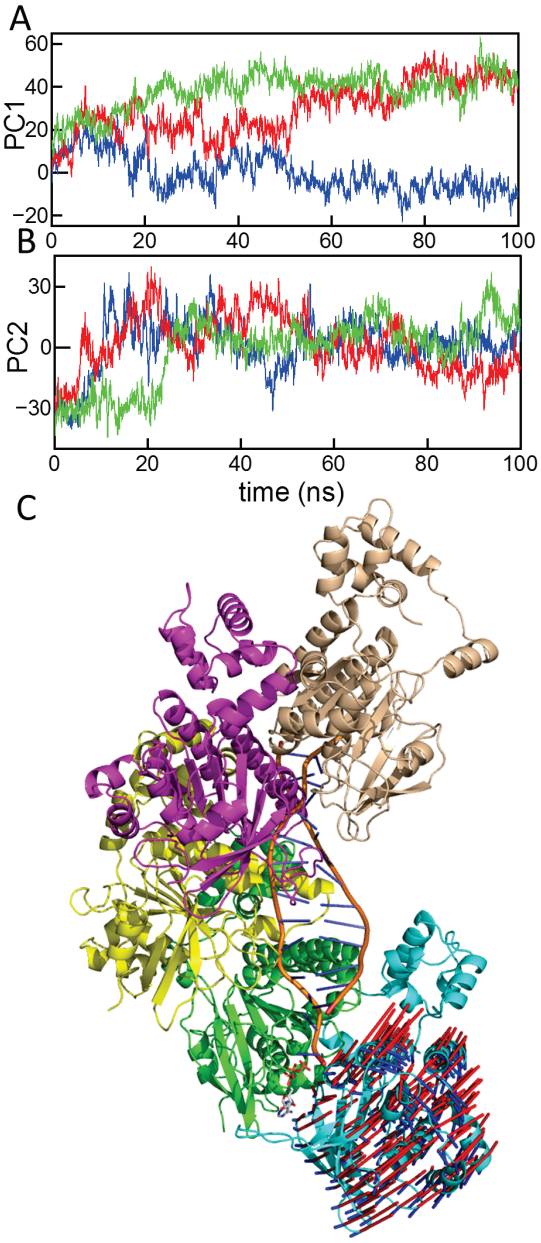

Figure S9. PCA for trajectories of the ADP-bound simulations in the second run. Projections of snapshots onto PC1 and PC2 during the $K^2N^{ATP}I^M$ (blue), $K^2N^{ADP+Pi}I^M$ (green), and $K^2N^{ADP}I^M$ (red) simulations are shown in panels *A* and *B*, respectively. The cosine contents of PC1 in $K^2N^{ATP}I^M$, $K^2N^{ADP+Pi}I^M$, and $K^2N^{ADP}I^M$ are 38 %, 29%, and 59 %, respectively. The cosine contents of PC2 in $K^2N^{ATP}I^M$, $K^2N^{ADP+Pi}I^M$, and $K^2N^{ADP}I^M$ are 4 %, 31%, and 14 %, respectively. In panel *C*, the directions of PC1 (red lines) and PC2 (blue lines) are shown (3 x square root of eigen values). The average dimer structure in $K^2N^{ATP}I^M$ was superimposed onto the terminal protomers of the crystal structure of the RecA-dsDNA filament. The bound ATP in the dimer was shown in stick representation.

Table S1. Summary of PROCHECK for the modeled structure and referenced crystal structure.

Residues except for L1 and L2 loops	Model	3LDA (Rad51)[1]
Most favored regions	98.0 %	92.2 %
Additional allowed regions	2.0 %	7.5 %
Generously allowed regions	0.0 %	0.4 %
Disallowed regions	0.0 %	0.0 %

Residues in L1 and L2 loops	Model	1XU4 (RadA)[2]
Most favored regions	76.7 %	53.3 %
Additional allowed regions	23.3 %	20.0 %
Generously allowed regions	0.0 %	13.3 %
Disallowed regions	0.0 %	13.3 %

[1]In the crystal structure (PDB ID: 3LDA), the L1 and L2 loops are missing.
[2]The L1 and L2 loops of the crystal structure (PDB ID: 1XU4) were referred to in the modeling.

Table S2. Charges in the vicinity of the ATP/GTP phosphate and Mg^{2+}. Charged residues within 6.5 Å of the phosphorus atoms of ATP/GTP and 5 Å of Mg^{2+} were listed. The threshold distance, 6.5 Å, was determined by taking into account the P-O distance of ~1.5 Å. The standard protonation state at pH 7 was used.

	Rad51	RadA	RecA	F_1-ATPase	Ras_RasGAP
PDB	Our model	1XU4	3CMW	2JDI	1WQ1
Positive charges	K^+(1), K^+(1), K191(1), R368(1), Mg^{2+}(2)	K^+(1), K^+(1), K111(1), Mg^{2+}(2),	K248(1)*, K250(1)*, K72(1), Mg^{2+}(2)	R373(1)*, K162(1), R189(1), R260(1), Mg^{2+}(2)	R789(1)*, K16(1), Mg^{2+}(2)
Negative charges	E221(-1), D280(-1), D374(-1), ATP(-4)	E151(-1), D211(-1), D302(-1), ATP(-4)	E96(-1), D144(-1), ATP(-4)	E188(-1), E192(-1), D256(-1), ATP(-4)	D57(-1), GTP(-4)
Total	-1	-2	-1	-1	-1

* These residues are in adjacent protomers.